Non-Invasive Personalisation of a Cardiac Electrophysiology Model from Body Surface Potential Mapping

Sophie Giffard-Roisin, Thomas Jackson, Lauren Fovargue, Jack Lee, Hervé Delingette, Reza Razavi, Nicholas Ayache, Maxime Sermesant

Non-Invasive Personalisation of a Cardiac Electrophysiology Model from Body Surface Potential Mapping

Sophie Giffard-Roisin, Thomas Jackson, Lauren Fovargue, Jack Lee, Hervé Delingette, Reza Razavi, Nicholas Ayache, Maxime Sermesant

***Abstract*—*Goal:* We use non-invasive data (body surface potential mapping, BSPM) to personalise the main parameters of a cardiac electrophysiological (EP) model for predicting the response to different pacing conditions. *Methods:* First, an efficient forward model is proposed, coupling the Mitchell-Schaeffer transmembrane potential model with a current dipole formulation. Then we estimate the main parameters of the cardiac model: activation onset location and tissue conductivity. A large patient-specific database of simulated BSPM is generated, from which specific features are extracted to train a machine learning algorithm. The activation onset location is computed from a Kernel Ridge Regression and a second regression calibrates the global ventricular conductivity. *Results:* The evaluation of the results is done both on a benchmark dataset of a patient with premature ventricular contraction (PVC) and on 5 non-ischaemic implanted cardiac resynchonisation therapy (CRT) patients with a total of 21 different pacing conditions. Good personalisation results were found in terms of the activation onset location for the PVC (mean distance error, MDE=20.3mm), for the pacing sites (MDE=21.7mm) and for the CRT patients (MDE=24.6mm). We tested the predictive power of the personalised model for biventricular pacing and showed that we could predict the new electrical activity patterns with a good accuracy in terms of BSPM signals. *Conclusion:* We have personalised the cardiac EP model and predicted new patient-specific pacing conditions. *Significance:* This is an encouraging first step towards a non-invasive pre-operative prediction of the response to different pacing conditions to assist clinicians for CRT patient selection and therapy planning.**

***Index Terms*—Cardiac Electrophysiology, ECG Imaging, Inverse Problem of ECG, Parameter estimation, Personalisation.**

I. Introduction

HEART Failure (HF) is a major health issue in Europe affecting 6 million patients and growing substantially because of the ageing population and improving survival following myocardial infarction. The poor short to medium term prognosis of these patients means that treatments such as cardiac resynchronisation therapy can have substantial impact [1]. However, these therapies are ineffective in 30% of the treated patients and involve significant morbidity and substantial cost. To this end, the precise understanding of the patient-specific cardiac function can help predict the response to therapy and therefore select the potential candidates and optimise the therapy.

In [2], Sermesant et al. proposed to personalize an electromechanical model of the heart to predict the response to CRT. The method requires to measure intra-cardiac electrical potentials through an invasive endovascular procedure which can be risky for the patient, and which is not suitable at a patient selection stage. The aim of this article is to extend this approach to non-invasive body surface potential mapping (BSPM), which uses up to 256 sensors on both sides of the torso, as the CardioInsight[1] jacket now commercially available. This has the potential to replace invasive measurements however the ability to estimate parameters and predict activation from such data still needs to be evaluated.

A. Cardiac EP Model Personalisation

Restricting our study to the ventricles, there are several types of EP models describing the action potential [3]; from complex ones (biophysical models) to very simplistic ones (Eikonal models). In this study we used the Mitchell-Schaeffer model [4] which is a phenomenological model of intermediate complexity with 2 variables and 6 parameters with a biophysical interpretation. From an onset activation location, the evolution of the transmembrane potential is computed at each node of a tetrahedral mesh of the myocardium using the finite element method.

The estimation of patient-specific parameters of a cardiac EP model is crucial for understanding of pathologies and predicting the response to therapies. The model personalisation usually deals with local parameters. [5] used optical mapping in an ex-vivo study to evaluate such algorithms. Personalisation using intra-cardiac potential mapping was investigated by [6]–[8], also including epicardial recordings. Calibration using non-invasive data was recently studied: [9] adjusted two parameters of an atrial EP model using BSPM data. [10] used two features from the 12-lead ECG to recover 3 electrical diffusivity parameters using a polynomial regression. The method is novel and efficient, but it suffers from the fact that the earliest activation site was fixed but actually unknown, and only two features (QRS duration and electrical axis) may not be sufficient to describe the cardiac activation. Such approaches have explored the use of machine learning for EP personalisation, but as no patient-specific database exists, they

S. Giffard-Roisin, H. Delingette, N. Ayache and M. Sermesant are with Asclepios Research Group, Université Côte d'Azur, Inria, France.

T. Jackson, L. Fovargue, J. Lee and R. Razavi are with Division of Imaging Sciences and Biomedical Engineering, King's College London, London, UK.

[1]ECVUE, CardioInsight Technologies Inc., Cleveland, Ohio

can only rely on simulated patient-specific samples covering the parameter space. In terms of personalisation methodology, [8] is based on an inference method combining polynomial chaos and compressed sensing, [10] employs polynomial regression into a statistical framework and [7] relies on a Bayesian inference model.

B. The Forward Problem of Electrocardiography

The estimation of the ECG data from the cardiac potentials is usually called the *forward* problem of electrocardiography (in opposition to the *inverse* problem, see I-C). The two classical numerical approaches are based either on the Boundary Element Method (BEM) or the Finite Element Method (FEM). They both propagate the epicardial heart action potentials to the surface of the body by taking into account the distance, the null current across the body surface, and the different properties of the tissues in between. Forward models differ also by their incorporation of heterogeneous conductivity regions associated with various organs within the torso. By taking into account the physical properties of the different tissues, the computed ECG account for more complex current pathways. In [11], Keller et al. demonstrates the importance of the torso inhomogeneity by ranking the influence of the different tissue conductivities on forward-calculated ECGs. Ramanathan et al. [12] showed, however, that at a first order approximation the torso inhomogeneities are not necessary for non-invasive reconstructions. Some techniques rely neither on BEM nor on FEM and assume a homogeneous and infinite torso domain using a dipole formulation [13]. While neglecting some the null current flow constraint at the body surface, it has been shown to be efficient on in-silico experiments.

C. The Inverse Problem of Electrocardiography

BSPM data has been widely used in the last decades to directly compute the cardiac action potentials by solving an ill-posed inverse problem: finding the transfer matrix linking the torso potentials to the cardiac potential sources [14]. If most of the methods are only estimating the potential on the surface of the heart (e.g. [15], [16]), transmural-based methods have been investigated in the last few years but are computationally more demanding [17], [18]. Rather than estimating directly the transmembrane potentials, the 3DCEI technique [19]–[22] solves the inverse problem by estimating the equivalent current density. Aside from standard regularization techniques, some inverse problem studies have been investigated imposing constraints in temporal and spatial domains [17], [23] or trying to take advantage of the space/time coupling of the electrical wave propagation [13], [24]. Some methods are also looking into integrating physiological and model-based priors in a Bayesian framework [25], [26]. The work by Li and He [27] solves the inverse problem by means of heart-model parameters (onset activation location) and was further extended [28] and validated on rabbits [29] and swines [30], [31]. A preliminary step is based on a priori knowledge using artificial neural network and an optimization algorithm refines the parameters. ECGI (Electrographic imaging) is already is commercially available, as the CardioInsight Technologies software [32] which was also used in recent ECGI studies [33]. ECGI can help in understanding dyssynchony and selecting CRT candidates : Varma et al. [34] and Ghosh et al. [35] worked on characterizing the EP substrate and electrical dyssynchony on HF patients undergoing CRT while Dawoud et al. [36] investigated regional electromechanical uncoupling in patients referred for CRT.

D. Proposed Approach

Our method is based on adjusting a forward model to measured BSPM in order to estimate patient-specific parameters and activation maps. Our personalisation involves identifying the parameters to predict new patient-specific pacing conditions. In order to avoid local minima we used a machine learning approach with the generation of a large patient-specific database of simulated BSPM. Some relevant shape descriptors were extracted from the simulated BSPM and used as patient-specific training set. We first learned the onset activation location using a Kernel Ridge Regression on activation maps, then use a second regression to calibrate the global ventricular conduction velocity. Because the onset activation is a local parameter, this method can be associated with a model personalisation. Our contributions are:

- A two-step algorithm that learns the parameters of the simulation by estimating the onset activation location and the global conduction velocity. The algorithm relies on machine learning approaches based on a few QRS shape-related features extracted from each BSPM sensor.
- A straightforward and efficient coupled forward model based on the Mitchell-Schaeffer model and on a current dipole formulation, allowing to simultaneously calculate transmural cardiac potentials and BSPMs. The Mitchell-Schaeffer model previously showed good predictive power in intra-cardiac studies [37].
- An evaluation (onset localisation and errors on the BSPM signals) on 52 different cardiac beats from 6 patients with 2 different types of pathologies: dyssynchrony and premature ventricular contraction. All the results were compared with standard inverse problem methods commercially available or other state-of-the-art methods, outperforming in a large majority of beats.
- A prediction of biventricular pacing activation maps and BSPM from personalised EP model parameters on 14 settings from 5 patients. Predicted BSPM are compared with measured BSPM.
- A quantification on the impact of myocardial geometry quality and scar tissue, and an extension of our method to standard 12-lead ECG data.

E. Outline of the Manuscript

In the following section II we will present our personalisation framework (Figure 1): clinical data, forward EP model and machine learning algorithm. Section III is dedicated to two evaluations on different datasets and to predictions of biventricular pacing. Finally, section IV discusses different aspects of the method, related in particular to the robustness and to the influence of the myocardial geometry and scar tissue.

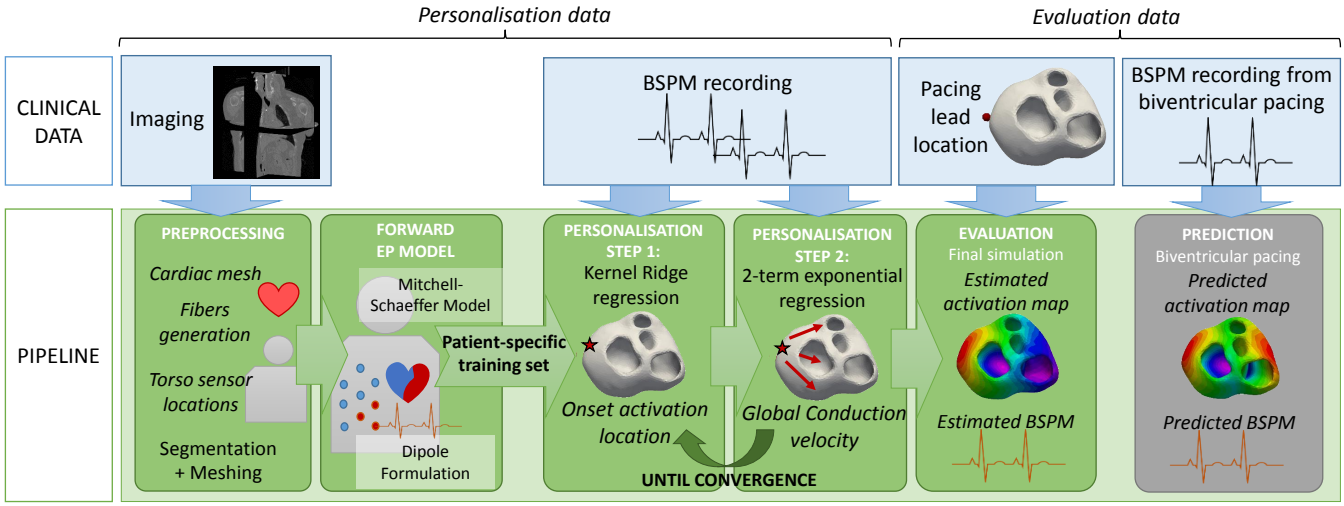

Fig. 1. Personalisation framework. Patient-specific geometrical data (section II-A) are used to build the coupled forward model (section II-B). Using Patient-specific training sets, the two-step personalisation (section II-C) based on machine learning techinques estimates the earliest activation location and the global conduction velocity from univentricular pacings or ectopic foci. The true location of the pacing lead is used for evaluation. A prediction of biventricular pacings (section III-C) is performed using estimated parameters from sinus rhythm personalisation.

II. Materials and Methods

A. Clinical Data

In this study, two datasets with different devices were used. The pacing lead is either at the tip of a moving catheter on the LV cavity or from a pacemaker device. The BSPM potentials were acquired during the procedure at a sampling rate of 1kHz, with different number of torso sensors depending on the device. The anatomy as well as the location of the torso sensors and the pacing leads were extracted either with imaging (MRI or CT scanner) or through the EP mapping system using magnetic sensors. Fibre orientations were estimated with a rule-based method (elevation angle between $-60°$ to $60°$). More details on the data will be provided in sections III-A1 and III-B1.

B. Simulating BSPM data: EP Forward Model

1) Mitchell-Schaeffer Cardiac Model: we simulated the electrical activation of the heart using the monodomain version of the Mitchell-Schaeffer's EP model [4]. It has two variables, the transmembrane potential v and z a secondary variable controlling the repolarization phase. Their evolution is governed by:

$$\begin{cases} \partial_t v = div(D\nabla v) + \frac{zv^2(1-v)}{\tau_{in}} - \frac{v}{\tau_{out}} + J_{stim} \\ \partial_t z = \begin{cases} \frac{1-z}{\tau_{open}} & \text{if} \quad v < v_{gate} \\ \frac{-z}{\tau_{close}} & \text{if} \quad v > v_{gate} \end{cases} \end{cases} \quad (1)$$

The parameters τ_{open} and τ_{close} define the gate opening and closing depending on the change-over voltage v_{gate}, and the parameters τ_{in} and τ_{out} control the depolarisation upstroke and repolarization downstroke. The diffusion term is defined by an anisotropic diffusion tensor $D = d \cdot diag(1, r, r)$ where d is the tissue electrical diffusivity. The anisotropy ratio r enables conduction velocity in the fibre direction to be larger than in the transverse plane (we used $r = (1/2.5)^2$).

The diffusivity d (in $m^2 s^{-1}$) can be expressed as a conductivity σ (in S/m) by using $\sigma = C_m \beta\, d$ with C_m the membrane capacitance and β the surface-to-volume ratio. From [38], we took $C_m = 10^{-2}\ F/m^2$ and $\beta = 10^5\, m^{-1}$. The local conductivity σ can be written in terms of intracellular and extracellular conductivities: $\sigma = \frac{\sigma^i \sigma^e}{\sigma^i + \sigma^e}$

The reduction of the monodomain model implies $\sigma^i = \lambda \sigma^e$ for some scalar λ resulting in a linear relationship between σ and σ^i. Finally, the diffusion d is linked to the conduction velocity c in m/s by $c = k\sqrt{d}$, where the constant k was estimated numerically in our simulations as $0.35\, s^{-1/2}$.

2) From Cardiac Simulations to BSPM, Current Dipole Formulation: we can compute simultaneously the cardiac electrical sources simulated in section II-B1 and the BSPM. As in [13], we modelled every myocardium volume element (tetrahedron) as a spatially fixed but time varying current dipole. We define the equivalent current density $\mathbf{j}_{eq}$ as:

$$\mathbf{j}_{eq} = -\sigma^i \nabla v \quad (2)$$

$\mathbf{j}_{eq}$ is a current dipole moment per unit of volume and the local dipole moment $\mathbf{p}$ in the volume V writes as $\mathbf{p} = \int_V \mathbf{j}_{eq} dV$.

The torso is composed of different organs that behave as different volume conductors. In a rough approximation, we consider an homogeneous, infinite volume of conductivity σ_T, and we took $\sigma_T = 0.2 S/m$. According to the volume conductor theory [39], the electric potential at a distance R in a homogeneous volume conductor of conductivity σ_T is:

$$\Psi(R) = \frac{1}{4\pi\sigma_T} \int_V \mathbf{j}_{eq} \cdot \nabla(\frac{1}{R}) dV \quad (3)$$

We model the moving propagation front as a dipole field. The infinitesimal dipole moment of the volume dV_X located at position X is defined as $\mathbf{p}_X = \mathbf{j}_{eq,X}\, dV_X = -\sigma^i_X\, \nabla v_X dV_X$. As we use linear tetrahedra in the FEM discretization of the myocardium, the potential v is linear and ∇v is constant over

the tetrahedron. We get the following formulation of the dipole moment of the charge in the volume V_H of tetrahedron H of the myocardial mesh: $\mathbf{p}_H = -\sigma^i_H \nabla v_H V_H$

The gradient of the electric potential ∇v_H for a tetrahedron H is estimated using the node positions X^k_H and the shape vectors $\overrightarrow{D^k_H}$ of the tetrahedron H [40]:

$$\overrightarrow{D^k_H} = \frac{s}{V_H}((X^{k\oplus 2}_H - X^{k\oplus 1}_H) \times (X^{k\oplus 3}_H - X^{k\oplus 1}_H) \quad (4)$$

where $s = 1$ for $k = 2, 4$, $s = -1$ for $k = 1, 3$, and $k \oplus l = (k-1+l) \mod 3+1$. The gradient of the electric potential in the tetrahedron H is then computed from the potentials $v(X^k_H)$ at the nodes X^k_H as:

$$\nabla v_H = \sum_{k=1}^{4} v(X^k_H)\overrightarrow{D^k_H} \quad (5)$$

From Equation 3, the contribution Ψ_H of the tetrahedron H to the potential field calculated at position X_T is:

$$\Psi_H(X_T) = \frac{1}{4\pi\sigma_T} \frac{\sigma^i_H V_H (\nabla v_H \cdot \overrightarrow{HT})}{\|\overrightarrow{HT}\|^3} \quad (6)$$

with $\overrightarrow{HT}$ the vector from centre of the tetrahedron H to the torso electrode location T. Finally, we sum over the whole mesh to get the potential field at X_T.

The implementation was done using the SOFA platform[2], with a direct coupling to the Mitchell-Schaeffer model. For a generic volumetric mesh of 65 000 vertices, every coupled simulation (cardiac model and dipole formulation) of 300 ms runs in less than 6 minutes, with a time step of 0.01 ms (using a dual-Xeon X5670 with 12 cores at 2.93GHz). With GPU version of the implementation [41], the simulation was performed in 2 minutes (using a dual-Xeon X5650 and a Tesla C2050 with 112 cores at 1.147 GHz).

3) Comparison of the Current Dipole Results with BEM: while being straightforward and efficient, this method includes some simplifications as the absence of a null current flow constraint at the body surface. To validate and estimate the errors of our forward model, we compared our results with a classical BEM forward formulation. We used the symmetric BEM from the OpenMEEG software[3] because it was shown to provide an excellent accuracy [42]. As input, the isolated dipole source were set at the center of each tetrahedra on the myocardium and calculated the vector sources of each tetrahedron at each time using Equation 2. We defined 3 domains: the myocardium, the torso and the air outside the torso (null conductivity). Their interfaces were defined using closed surface meshes. The linear operator L which associates dipolar sources to the resulting sensor measurements is calculated by solving $L = S\,G^{-1}\,D$, where D is the dipole matrix, S is the sensor matrix and G is the geometry matrix. With a torso surface mesh of 4K vertices, a heart surface mesh of 7K, 75K dipolar sources and 52 sensors, the L matrix is computed in 7 hours. As an example, the potentials at 4 random sensor locations simulated with OpenMEEG (blue) and our dipole formulation (red) are shown in Figure 2. In some surface potentials the OpenMEEG ECG has larger amplitude as on b and c, whereas on some other the amplitude is lower as on a and d. The difference is due to the absence of boundary conditions in our formulation. A key point to notice is that the signal shape and sign are similar, while reducing the computation time from 7 hours to a few minutes.

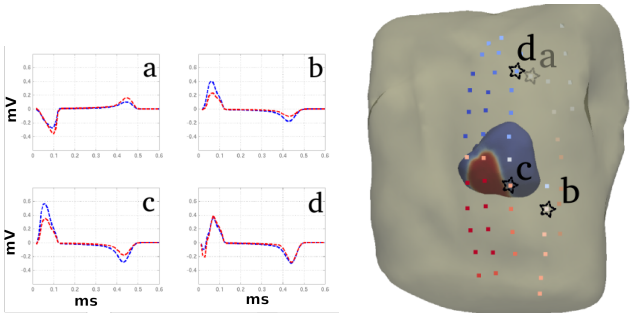

(a) (b)

Fig. 2. (a) Body surface potentials over one cardiac cycle (4 examples): OpenMEEG (blue), dipole formulation (red). (b) positions of the 4 sensors on the torso, the sensor **a** is on the back.

C. Personalising a Cardiac EP Model from BSPM

1) A Two-step Machine Learning-based Personalisation: The two machine learning algorithms are two different regressions, both using simulated patient-specific data as training sets.For the first step, a Kernel Ridge Regression is estimating the onset activation location. From 250 random onset activation locations, their respective activation maps are simulated together with their simulated BSPM. After a feature extraction on both the measured and the simulated BSPM, the Kernel Ridge Regression estimates the cardiac activation time corresponding to the measured BSPM on each node of the cardiac mesh from the cardiac activation times of the simulated BSPM with the closest features. The onset location is identified as the node with the smallest activation time. During the second step, 100 conduction velocity values and their simulated BSPMs are used as a training set for a two-term exponential regression. Once the unknowns of the regression function are estimated, the conduction velocity of the true signal is estimated (see Figure 1).

2) BSPM Feature Description: important aspects of the torso electrical signal are the shape, the timing and the sign of the QRS complex. Because the reference electrode is often not localized, each signal (measured and simulated) was first subtracted by the mean BSPM signal (measured or simulated). Then each signal (measured or simulated) was normalized and smoothed with a local Gaussian filter. We then defined $7 \times n_s$ descriptors (n_s being the number of sensors in the jacket) of the QRS window as (see Figure 3): (1) timing of the global extremum, (2) absolute potential of the global extremum, (3) sign the global extremum, (4) number of zero crossings, (5) number of local extrema, (6) relative algebraic area, (7) sign of the first extremum. This choice was inspired by previous works on ECG analysis, e.g. [43].

[2]SOFA is an Open Source medical simulation software available at http://www.sofa-framework.org

[3]OpenMEEG is an Open Source software that solves problems related to EEG and MEG, available at http://openmeeg.github.io.

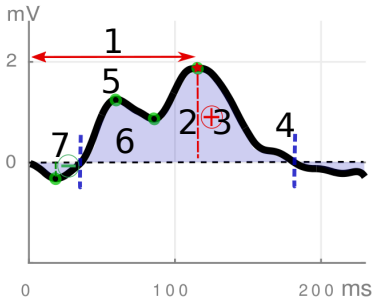

Fig. 3. Example of BSPM for one sensor. The extracted features are the position of the global extremum (1: red arrow),the absolute potential of the global extremum (2: red bar), the sign of the global extremum (3: red sign), the number of zero crossings (4: blue lines), the number of local extrema (5: green dots), the algebraic area (6: blue), the sign of the first extremum (7: green sign).

3) First Step, Locate the Activation Onset with Kernel Ridge Regression: the shape of the measured torso signals strongly depends on the position of the onset activation. The first step of the non-invasive cardiac model personalisation is an automatic estimation of the onset activation site on the cardiac mesh. From a list of 250 random nodes on the surface of the cardiac mesh (epicardium and endocardium), we simulated a set of activation maps and corresponding BSPM. We fixed the global ventricular conduction velocity to a nominal value of $0.5\,m.s^{-1}$ and we only used the 6 features that are invariant to a small change of the global conduction velocity (i.e. we excluded the timing of the global extremum). The training feature database was normalized along each feature. We used a Kernel Ridge Regression between features extracted from the BSPM to predict the activation time on each node of the cardiac mesh. A Ridge Regression is a regularized least square method which is suited for a reasonable number of training examples. The kernel trick is useful here because the number of features (roughly 1500) is larger than the number of samples (250). We simulated a database composed of 250 couples (x_i, y_i) of feature vectors x_i and corresponding depolarization time vectors y_i. The predicted target y for a new test point x was estimated using:

$$y = \mathbf{y}(K + \frac{1}{\gamma}\mathbf{I}_n)^{-1}\kappa(x)$$

where $\mathbf{y}$ is the matrix of the sampled targets y_i, $K(x_i, x_j) = exp(-(x_i - x_j)^2/\sigma^2)$ is a Gaussian kernel of bandwidth σ, and the i-th coordinate of the vector $\kappa(x)$ is defined as $(\kappa(x))_i = K(x_i, x)$. γ is the coefficient balancing the smoothness and the adherence to the data. The tuning of σ and γ was performed by a ten fold cross-validation. The same values were used for other patients. For each couple of parameters (σ, γ) the mean distance to the synthetic onset location is plotted in Figure 4a. It represents the error, since a perfect initial position estimate would result in a null distance. The estimated prediction error is $5.7mm$ for the couple $(\sigma = 10^{3.5}, \gamma = 10)$. We notice that the value of σ is of the same order of magnitude as the size of the feature vector x_i. This is coherent, because each component of x_i belongs to a distribution with unitary standard deviation, so the distance between x_i and x_j is also of the order of their size. Figure 4b shows the distance error to the true pacing location for a clinical case when varying dataset size (result unchanged after 200 samples).

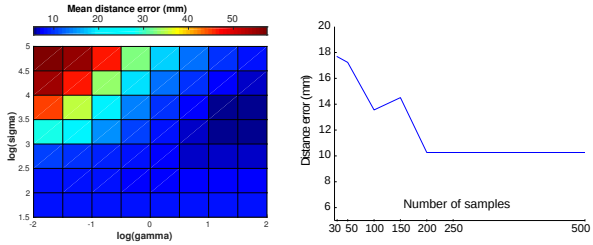

(a) (b)

Fig. 4. First Step. (a) Cross-validation: error in terms of mean distance to the synthetic true initial activation when varying the two parameters of the Kernel Ridge Regressor. (b) Distance error to the true onset for one clinical case with respect to the size of the database (retained size is 250 samples).

4) Second Step, Estimate the Ventricular Cardiac Conduction Velocity with Two-term Exponential Regression: the previous estimation of the onset location allowed us to further calibrate the EP model. We modelled the ventricles as an homogeneous tissue with a uniform conduction velocity (CV) that we want to estimate. We randomly sample 100 CV in the range $[0.2, 1.5]m.s^{-1}$. We generated the corresponding personalised BSPM database with fixed onset location. We extracted from the simulated BSPM one type of feature directly related to the CV: the position of the global extremum. The size of one feature vector is thus $1 \times n_s$, and the database was composed of 100 couples (x_i, y_i) of feature vectors x_i and corresponding CV parameters y_i. The predicted target y for a new test point x was estimated by a regression between the first mode of the PCA of the training feature vectors $X_{1,i}$ and the conduction velocities y_i. The estimated function $f(X_1) = y$ was fitted using a two-term exponential regression:

$$f(x) = ae^{bx} + ce^{dx} \tag{7}$$

In some cases, a too small conductivity can make the extremum of the signal exceed the QRS time frame; so the corresponding samples were automatically excluded. Finally, the measured BSPM can be projected into the PCA space and the CV is estimated from the regression (Figure II-C4).

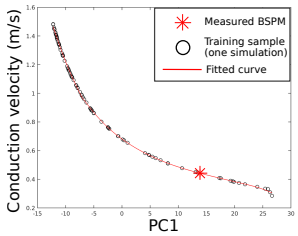

Fig. 5. Second Step. Example for one patient and one pacing. 2-term exponential regression using the first principal component with automatic exclusion of outliers (small conductivities). The red star is the measured BSPM projection.

5) Iterating and Final Simulation Using Estimated Parameters: step 1 and 2 are then iterated until convergence ($\Delta c < 0.05m/s$). The final step consists in re-running the EP model during one cardiac cycle using the estimated onset

location and the estimated global CV. The final result consists in a transmural activation map, where the depolarisation times are computed at each node of the mesh. In addition we simulate the corresponding BSPM. An estimation of the result confidence is given by the averaged correlation coefficient (CC) between the simulated and measured BSPM.

III. Personalisation Experiments and Results

A. Evaluation on PVC Benchmark Clinical Dataset

1) BSPM and Intracardiac Acquisitions: we tested our method on a benchmark study of the ECGI community which provides clinical data from 63 BSPM electrodes on one non-ischaemic patient recorded during an Premature Ventricular Contraction (PVC) ablation procedure. Ventricularly paced beats from a catheter were also recorded. The dataset[4] includes the geometry of the myocardium, the location of the 63 torso electrodes and the 7 pacing sites, as well as an estimation of the PVC site, see Figure 6. For the PVC ground truth, both the earliest measured local activation time measured by intracardiac CARTO system and the latest successful ablation site were recorded: they do not match but they both give an indication about the real PVC location. The BSPMs consist in several QRS time windows at a sampling rate of 1kHz. The QRS without pacing (marked as 'PVC') was recorded 10 times (10 runs), while for the 7 pacing sites the number of runs varies from 1 to 14. A volumetric myocardial mesh of roughly 10K elements was created from the provided surface mesh using the CGAL[5] meshing software, and fibre directions were estimated (see Section II-A).

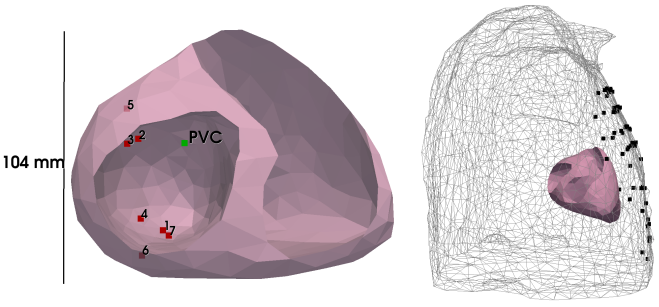

(a) (b)

Fig. 6. PVC data geometry. (a) myocardial mesh with measured pacing locations (red) and PVC location as the earliest activation time measured (green). (b) 64 BSPM electrodes (black), myocardial mesh (pink).

2) Results for PVC and Pacing Sites Localisation: our personalisation pipeline was launched for every run, and we compared the localization errors with those of the inverse method of [44]. Figure 7a presents the error distances for the PVC (mean distance error or $MDE = 20.3mm$) and for 7 catheter pacing locations ($MDE = 21.69mm$ among all pacings). The error distances have to be compared to the distance of the measured excitation onset point to the closest point of the mesh ($11.8mm$ for the PVC, pink dotted line), showing that the registration between the intra catheter localisation and the pre-operative imaging is not very accurate. From Figure 7a, our personalisation method provides results comparable to other state-of-the art inverse problem methods like [44], with better results for a majority of pacing sites locations. Global CV for all PVC runs was found in the range $[0.33, 0.38]m/s$. Looking at Figures 7b and 7c, the estimated PVC location is found to be close to the location of the earliest activation time measured and the latest successful ablation site lying in the aorta. The former was measured by catheter, while the latter is the location where the ablation procedure succeeded.

[4]This dataset was provided by the Institute of Biomedical Engineering, Karlsruhe Institute of Technology (KIT), Germany and the First Department of Medicine (Cardiology), University Medical Centre Mannheim, Germany.

[5]CGAL is a Computational Geometry Algorithms Library, available at www.cgal.org

TABLE I
CRT patients. Baseline information of the 5 patients treated.

Id	Age	Gender	Sinus rhythm	MRI	Presence of scar
1	82	M	X		
2	49	F	X		
3	87	M			
4	69	F			
5	49	M	X	X	X

B. Evaluation on Five Implanted CRT Patients

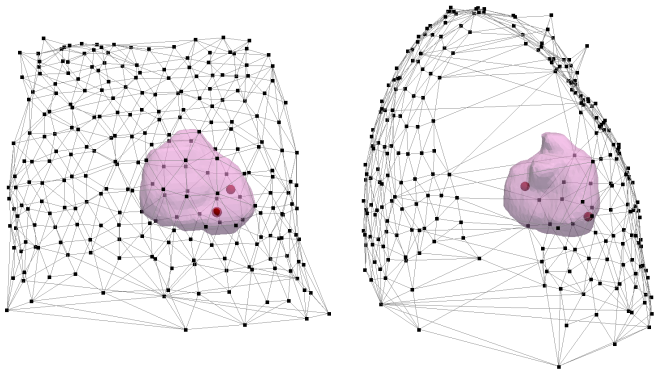

Fig. 8. CRT patients geometry. CardioInsight geometries from hand segmentation of CT image: Torso sensors (black dots), left and right pacing sites (red), epicardial surface (pink).

1) BSPM Acquisitions with CardioInsight Jackets: The second dataset was acquired at St Thomas' Hospital, London. The CardioInsight jacket is able to acquire simultaneously 256 signals on the torso surface. The dataset consists of 5 patients, all being implanted CRT patients and non ischaemic. In the optimisation procedure, the cardiologists performs several recordings corresponding to different pacing combinations and delays between the right ventricle (RV pacing, endocardial) and the left ventricle (LV pacing, epicardial) pacing leads. In total, 114 different settings were recorded. For all patients, an LV pacing and an RV pacing were performed, together with several biventricular pacings where the two stimulations are either simultaneous or separated by a delay. A sinus rhythm sequence is also recorded on patients that do not have complete

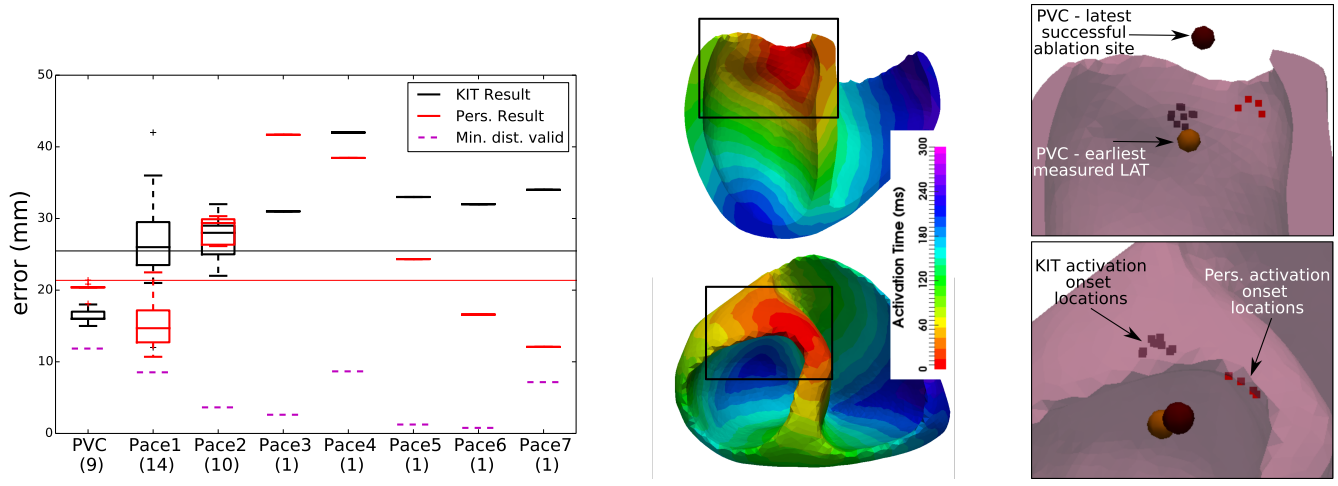

(a) (b) PVC (c) PVC

Fig. 7. PVC results. (a) Error distances (mm) of estimated onset location to the measured location by the CARTO system for the PVC (9 runs) and to the catheter pacings for the 7 pacing sites of Figure 6 (29 runs in total). Comparison between our personalisation and the KIT inverse method. 'Minimal distance valid': distance of the measured excitation origin to the closest point in the mesh. Mean values are represented by the lines. (b) Personalised PVC transmural activation map. (c) Long and short axis zooms showing the estimated 9 PVC activation onset locations from KIT (black) and from our personalisation (red). Ground truth is taken as the earliest measured local activation time (brown). The latest successful ablation site (dark brown) was found in the aorta.

heart blocks, see Table I. The QRS time window was recorded at a sampling rate of 1kHz. From the information given on the state of every sensor (*good, disconnected, missing, bad*), the non reliable sensors of each recording was removed. The number of sensors used in our personalisation varied between 175 and 220.

The relative position of electrodes and pacing sites with respect to an epicardial geometry were hand-extracted from a CT scanner performed the day of the intervention (Figure 8). Important artifacts on the CT scanner coming from the pacemaker prevents creating a better segmentation. The CardioInsight Technologies software is solving the inverse problem on this epicardial surface. The method estimates the epicardial potentials based on the standard formulation using a Tikhonov regularization and the generalized minimal residual algorithm [32]. Clinicians can use the activation maps from the CardioInsight software for diagnosis or therapy planning. In this work, we used these activation maps to evaluate our personalisation algorithm.

For patient 5 the precise geometry of the heart was extracted using Magnetic Resonance Imaging (MRI), allowing us to segment properly the myocardium. In addition, delayed contrast enhancement MRI (DCE-MRI) was also acquired and a scar region was segmented (patient 5 has a non-ischaemic cardiomyopathy, NICM). The other patients with recorded BSPM did not undergo MRI as they were already implanted (Table I). We used this patient to evaluate the effects of the precise myocardium geometry and the presence of scar tissue.

2) Pre-processing: for Patient 5, the myocardial mesh was generated using the VP2HF [6] platform and the VP2HF meshing pipeline [45] creating a tetrahedral mesh with roughly 150K elements. The scar was semi-automatically segmented by a clinician and registered to the myocardial mesh. We imposed the scar tissue to have no reaction term in the Mitchell-Schaeffer model by setting much higher values of τ_{in} and τ_{out} (cf. Eq. 1) and a small conduction velocity of $0.2m/s$. We manually rigidly registered this volumetric mesh to the epicardial surface extracted from the CT scanner. For other patients, as no precise geometry was available a generic volumetric myocardial mesh of roughly 65K tetrahedra was manually registered to the CT image. Even if the shape of the myocardium is generic, its orientation, its position and its size is patient-specific.

3) Error on Onset Activation Location: Figure 9 shows for the 5 patients the Euclidean distance between the onset activation location and the true pacing lead. For all patients, 3 iterations were necessary and the mean improvement in terms of localization error was 2mm. The CardioInsight onset location is constrained to lie on the CardioInsight epicardial mesh whereas our method constrain it to lie on the volumetric mesh (but often generic), so both models include geometry uncertainties. The MDE for both LV and RV pacings were found at $24.6(std = 11.9)mm$ for our personalisation results, and $39.3(std = 15.8)mm$ for the CardioInsight inverse solution. Patient 2 has very poor data quality (obese person with 20% of torso sensors disconnected and located in the sensitive zone) explaining the poor result in terms of localization by the personalisation (43mm for RV/LV) as well as by CardioInsight (RV:62mm, LV:52mm).

4) Results on Conduction Velocity: The estimated CV could not be quantitatively evaluated because the ground truth is not available but we can look at the coherence between several acquisitions with different pacing conditions for the same patient. Figure 10 shows the CV values for the sinus rhythm, the LV pacing and the RV pacing. We can see that based on a broad range of possible values (uniformly in [0.2,1.5]m/s), all CVs lie within a clinically acceptable range ([0.29,0.62]m/s) [46]. Moreover, the global CV found with different pacing

[6]VP2HF is a European Seventh Framework Program, http://www.vp2hf.eu

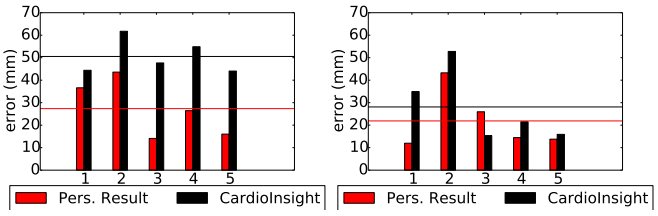

(a) RV pacing (b) LV pacing

Fig. 9. CRT patients. Error distances of estimated onset location to the true pacing lead position for every patient. Comparision of the proposed personalisation (red) to the CardioInsight inverse solution (black). The means (med) are represented by the lines.

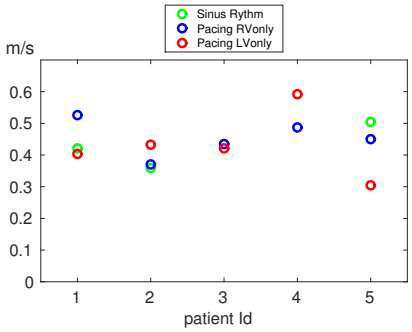

Fig. 10. CRT patients. Estimated conduction velocity for every patient, using the LV pacing (red), the RV pacing (blue) and the sinus rhythm (green) when available.

locations on the same patient are usually in good agreement.

5) Comparison of the Estimated Activation Maps: Figures 11a, 11c, 11e show for Patient 5 the estimated transmural activation maps obtained after our personalisation for the sinus rhythm, the RV pacing and the LV pacing. The red dot indicates the true pacing lead position as segmented from the CT scanner. The early activation zones were found near the true pacing lead. We are also showing the CardioInsight epicardial solution (Figures 11b, 11d, 11f). If the comparison shows a good agreement, on this case our personalisation gives a more precise solution. For example, we can see that the sinus rhythm onset was found on the septum, which is not visible in the CardioInsight solution.

6) Results in terms of BSPM signals: the simulated and the measured BSPMs of patient 5 are represented in Figure 12 for 6 sensors uniformly chosen. The simulated BSPM has been scaled by its total norm and multiplied by the measured BSPM total norm. We calculated for each recording the averaged CC between measured and estimated BSPM. We can see a good agreement for the RV pacing and the LV pacing, while the signals of the sinus rhythm are more difficult to reproduce for this patient ($\overline{CC} = 0.32$). It may be due to the fact that this sinus rhythm sequence is complex (presence of scar, possibly multiple onsets). For the two other sinus rhythm personalisations (patients 1 and 2) we found a better agreement with a $\overline{CC}$ of 0.58 and 0.62. Figure 13 depicts the evolution of the estimated signal during the different steps of our personalisation for the RV pacing. The averaged CC is improved after each step (from -0.15 to 0.83).

C. Prediction of Stimulation Results from Personalised Model

While our approach does provide an activation map of the myocardium, the main aim of this personalisation is to benefit from the predictive power of the underlying forward model. We therefore tested in this section how well the personalised models could predict different pacing conditions. To this end, we used the CV results of our personalisation from the sinus rhythm (estimated in section III-B4) to simulate biventricular pacing (when the sinus rhythm was not available, we took the mean of the LV pacing and RV pacing). In the clinical procedure several types of biventricular pacings were tested by changing the timing between the two stimuli. The 3 classical combinations are: simultaneous pacings; LV stimuli ahead by 40 ms (LV40); RV stimuli ahead by 40 ms (RV40). Results are shown on Figure 14 for the RV40 of Patient 5 and for the LV40 of Patient 4, indicating a reasonably correct prediction in terms of BSPM shape, timings and averaged CC.

IV. Discussion

A. Personalisation using 12-lead ECG data

From the BSPM electrodes of the CRT dataset, we extracted for each patient 9 electrodes roughly located at conventional ECG placement in order to derive the 12-lead ECG (Figure 15). The derivations were performed on the simulated and on the ground truth signals. We applied our personalisation for the 12-lead ECG data to the 5 CRT patients. The MDE was $29.8mm$, which is higher than the BSPM personalisation ($24.6mm$). However by looking closely at the results, the errors were particularly important on patient 2 (RV lead: $57mm$, LV lead: $64mm$), while small errors were obtained on patient 5 (RV lead: $10mm$, LV lead: $12mm$). Knowing that the data from patient 2 was of very poor quality and that patient 5 is the only one having a personalised geometry, the 12-lead ECG may be less robust than BSPM personalisation. The fact that the location was well located on cases with correct data quality seems to show that our method is sufficiently constrained such as to work with few signals.

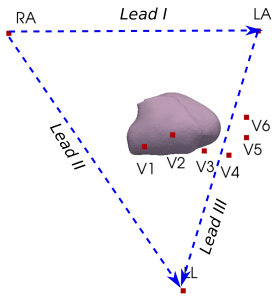

Fig. 15. Comparison with 12-lead ECG data. The 9 electrode locations used for the derivation of the 12-lead ECG are taken from the BSPM electrodes.

B. Quantifying the Impact of a Precise Myocardial Geometry

Only the data from Patient 5 of the CRT database included MRI and thus allowing a precise myocardial segmentation. For other patients, a generic heart mesh was rigidly registered

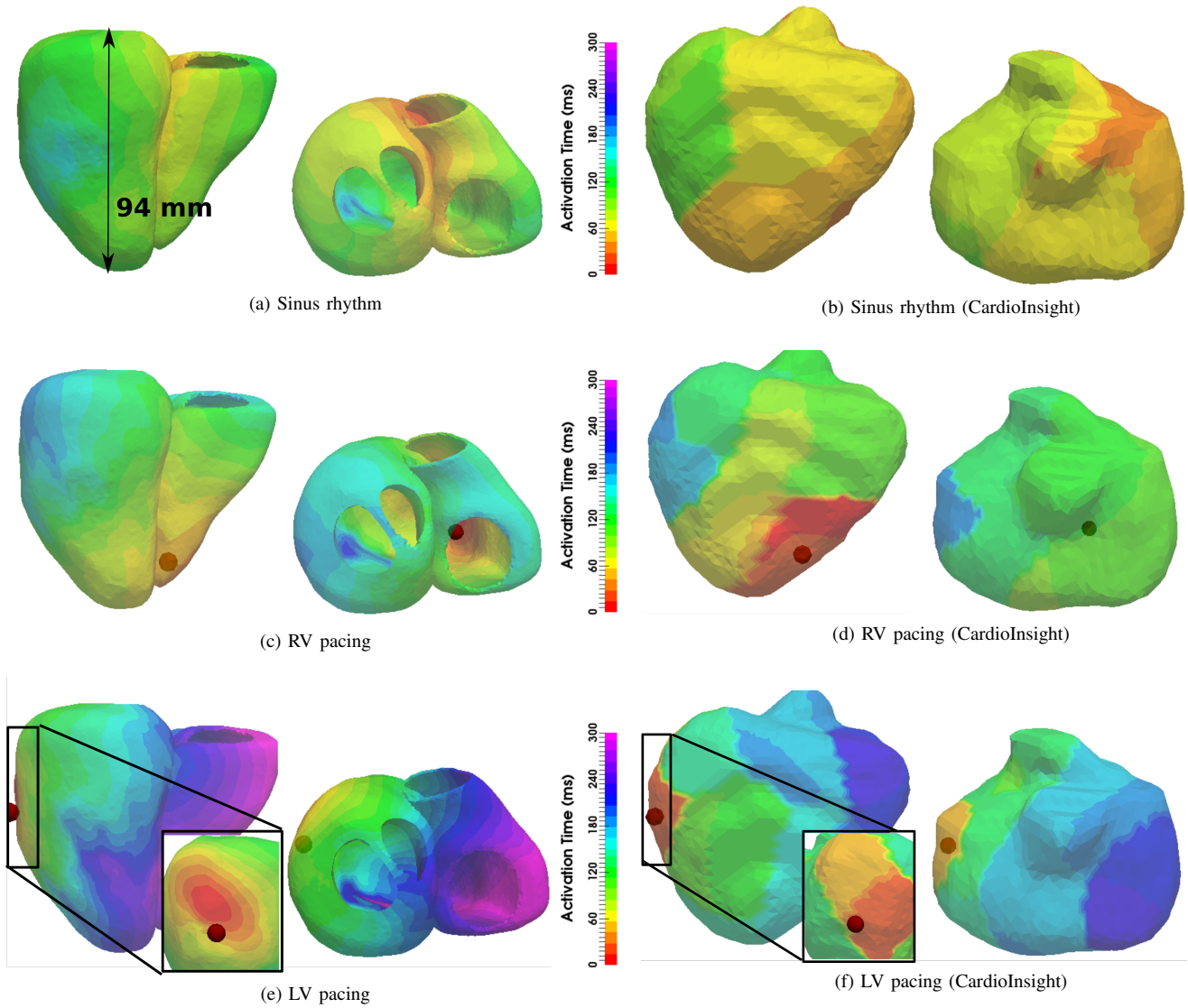

(a) Sinus rhythm

(b) Sinus rhythm (CardioInsight)

(c) RV pacing

(d) RV pacing (CardioInsight)

(e) LV pacing

(f) LV pacing (CardioInsight)

Fig. 11. CRT Patient 5 activation maps, the red dot corresponds to the true pacing lead position. (a)(c)(e) Our personalisation result (transmural), (b)(d)(f) CardioInsight solutions (epicardial). (a)(b) Sinus rhythm, (c)(d) RV pacing and (e)(f) LV pacing.

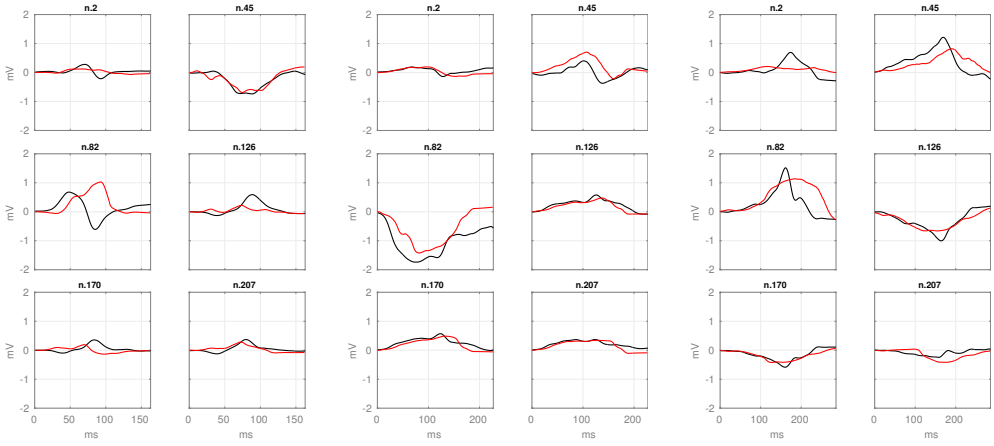

(a) Sinus rhythm ($\overline{CC} = 0.32$)

(b) RV pacing ($\overline{CC} = 0.83$)

(c) LV pacing ($\overline{CC} = 0.48$)

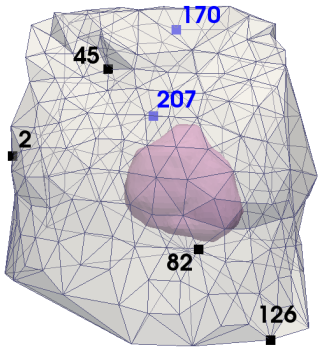

(d)

Fig. 12. CRT Patient 5. Example of 6 BSPM sensors of the QRS measured (black) and personalised (red) in mV per ms. (a) Sinus rhythm (b) RV pacing only (c) LV pacing only. The averaged correlation coefficient are indicated below. (d) Locations of the 6 chosen BSPM sensors, the blue ones are on the back.

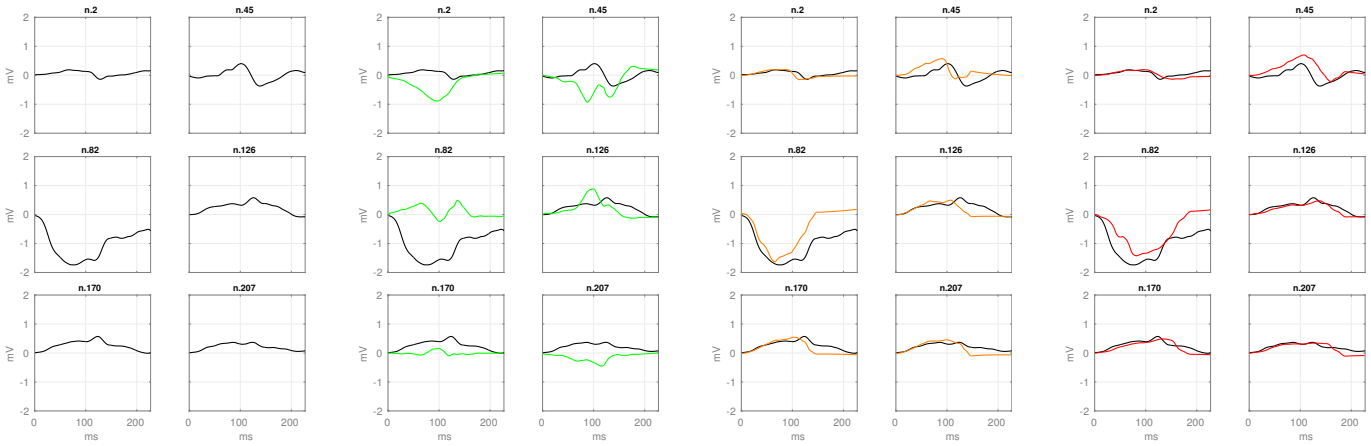

(a) Measured (b) After preprocess($\overline{CC} = -0.15$) (c) After step 1 ($\overline{CC} = 0.65$) (d) After step 2 ($\overline{CC} = 0.83$)

Fig. 13. CRT Patient 5. Example of 6 BSPM sensors for the RV pacing in mV per ms. (black) QRS measured. (green) Pre-processing: simulated QRS using patient-specific geometry with random onset location. (orange) Step 1: simulated QRS after activation onset location estimation. (red) Step 2: simulated QRS after CV estimation. The averaged correlation coefficient are indicated below.

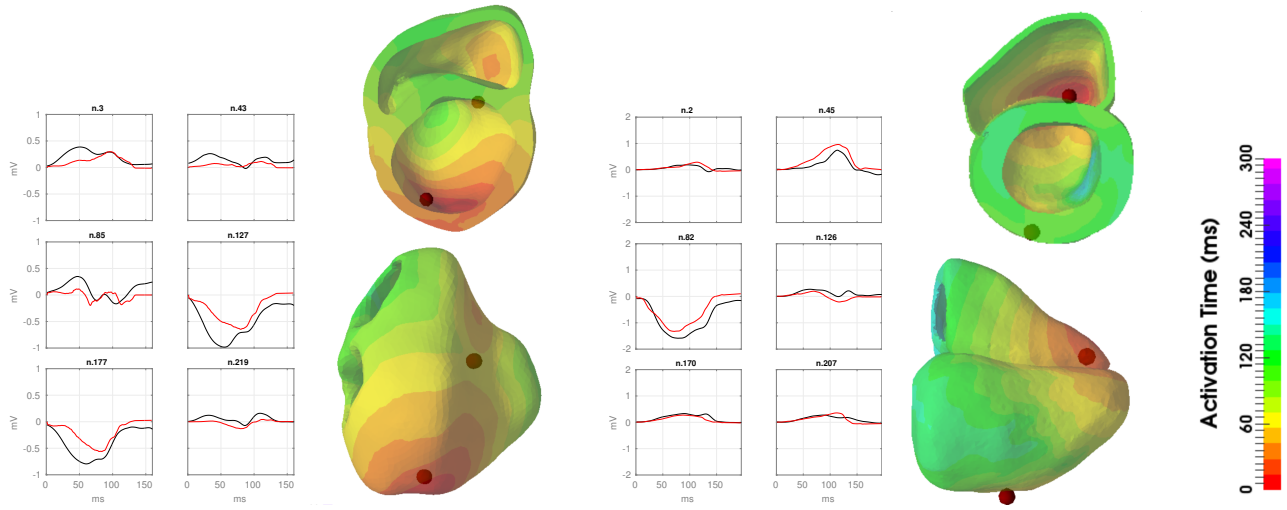

(a) $\overline{CC} = 0.70$ (b) (c) $\overline{CC} = 0.61$ (d)

Fig. 14. CRT Patients 4 and 5: predictions. (a)(b) Patient 4: biventricular pacing with LV lead ahead by 40ms, using the parameters estimated by our personalisation of the LV only and RV only. (a) example of 6 BSPM sensors of the QRS measured (black) and estimated (red). (b) activation map (generic mesh). (c)(d) Patient 5: biventricular pacing with RV lead ahead by 40ms, using the parameters estimated by our personalisation of the sinus rhythm. (c) example of 6 BSPM sensors of the QRS measured (black) and estimated (red). (d) activation map. The red dots corresponds to the true pacing lead positions.

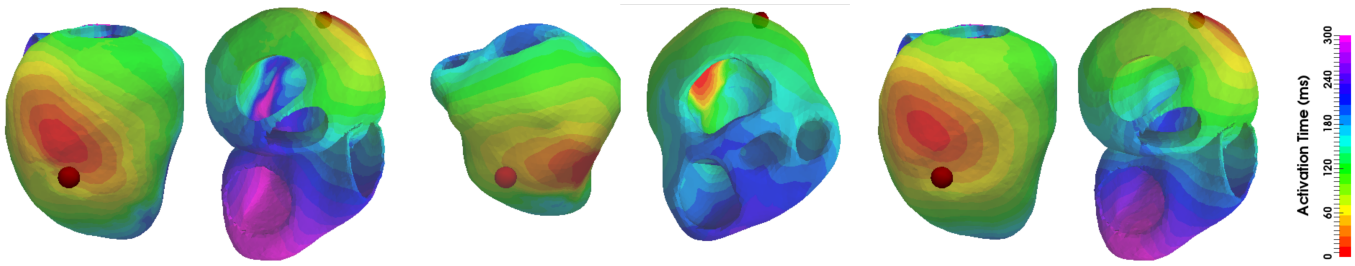

(a) LV pacing (b) LV pacing (generic mesh) (c) LV pacing (no scar)

Fig. 16. CRT Patient 5 estimated activation maps for LV pacing, the red dot corresponds to the true pacing lead position. (a) Result with a personalized geometry and scar (same as Figure 11e), (b) result with a generic geometry and scar, (c) result with a personalized geometry but no scar.

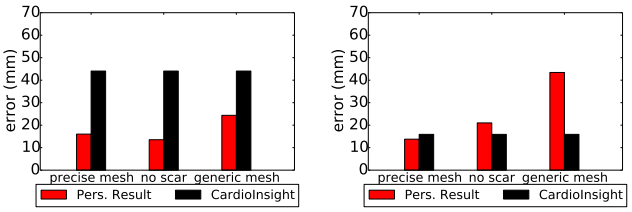

(a) Patient 5 : RV pacing (b) Patient 5 : LV pacing

Fig. 17. CRT patient 5. Onset location distance error. Result with a personalised geometry and scar, result with a personalised geometry but no scar and result with a generic geometry and scar.

and scaled to the myocardial shape from a CT scanner with important artifacts. In this section we want to quantify the impact of a precise myocardial geometry to our personalisation results in terms of onset location and errors on BSPM. The results of patient 5 using the MRI segmentation were compared to the results using the generic heart manually rigidly registered and scaled to the same location. Since Patient 5 has a scar segmentation available (see Section III-B2), the scar region was also mapped to the generic heart mesh. From Figure 17, the onset location was found to be less accurate with the generic mesh for the LV pacing (error is 43.4mm for the generic heart, 13.7mm for the MRI segmentation) as well as for the RV pacing (24.3mm for the generic heart, 16.0mm for the MRI segmentation). The activation map using the generic mesh for the LV pacing can be seen in Figure16b. We can notice that the estimated onset locations using a generic heart are still in an acceptable error range. We can conclude that a patient-specific geometry leads to a more accurate personalisation while the use of a generic mesh is still a fair approximation on this case.

C. Modelling Scar Tissue: Its Impact on our Personalisation

The 6 patients from both datasets were identified as non-ischaemic. However, patient 5 has a NICM with an annotated scar from DCE-MRI. In the presence of scar tissues we suppress the reaction term in the Mitchell-Schaeffer model and reduce the conductivity of the tissues to $0.2m/s$. In order to measure the impact of a scar on the personalisation process, we compared in Figure 17 the precision obtained with and without the scar information. We can see that including the scar information yields better results for the LV pacing, where the pacing lead is closer to the scar region (see Figure 16c for the estimated activation map). By incorporating some structural information, we were able to improve the personalisation results. However, as the scar information is not always available we believe that it could be learned directly through the personalisation process, by detecting regions where the conductivity has to be locally reduced.

D. Future Works

We have been estimating the parameters of singular pacing sites and predicting the response to multiple pacings. We are now interested in extending the study to the estimation of the location of more than one activation site, and we believe it would only require more computation time for increasing the training database. A future goal is to help the clinicians in predicting the best combination and the best lead locations among the possible and reachable zones before the implantation. As the work by Swenson et al. [47] reveals the importance of the cardiac position in the ECG forward problem, we believe that a more precise registration of the myocardial mesh to the CT scanner would have a positive impact. Finally, in this study we did not include a Purkinje system model as most of the patients have bundle branch blocks, but we believe it to be an important improvement. To account for more drastic variations of onset and conductivities, we may also reconsider the methodology as the use of advanced non-linear dimensionality reduction techniques. Even if the current difficulty of the personalisation is to understand and model to complex pathologies, we do think that it could help the analysis of ECGI because the problem is more physiologically constrained.

V. Conclusion

From non-invasive measures including BSPM signals, we were able to personalise the location of the onset activation location and the global conduction velocity of the myocardium with a two-step algorithm. We built a large database of simulated BSPM in order to train a machine learning algorithm based on a few QRS shape-related features from each BSPM sensor. The simulated BSPM relies on a transmural forward model based on the Mitchell-Schaeffer model and a current dipole formulation. We validated our approach on a PVC localisation ($MDE = 20.3mm$), on 29 runs from 7 pacing sites by catheter ($MDE = 21.6mm$) and on 10 different pacing sequences from 5 CRT patients ($MDE = 24.6mm$). A comparison with two standard inverse methods revealed that our personalisation provides comparable results. We also showed that we were able to predict the response to biventricular pacings based on our personalised models with concordance in the BSPM signals. Finally, we showed on limited cases that personalised scar and myocardial geometry improved the results and we studied the extension of our method to standard 12-lead ECG data. This is an encouraging first step towards a pre-operative prediction of different pacing conditions in order to assist clinicians for CRT decision and procedure.

Acknowledgment

The research leading to these results has received funding from the Seventh Framework Programme (FP7/2007-2013) under grant agreement VP2HF n°611823. This research contributes to the objectives of the ERC Advanced Grant MedYMA (2011-291080). We also thank Nicolas Duchateau, the Consortium for Electrocardiographic Imaging (CEI) (in particular Walther Schulze, Danila Potyagaylo and Olaf Dössel) for making public the PVC dataset and Maureen Clerc and Theo Papadopoulo for their help with the OpenMEEG library.

References

[1] M. G. S. J. Sutton *et al.*, "Effect of cardiac resynchronization therapy on left ventricular size and function in chronic heart failure," *Circulation*, vol. 107, no. 15, pp. 1985–1990, 2003.

[2] M. Sermesant *et al.*, "Patient-specific electromechanical models of the heart for the prediction of pacing acute effects in crt: A preliminary clinical validation," *Medical image analysis*, vol. 16, no. 1, pp. 201–215, 2012.

[3] A. E. Pollard, "From myocardial cell models to action potential propagation," *Journal of electrocardiology*, vol. 36, pp. 43–49, 2003.

[4] C. C. Mitchell and D. G. Schaeffer, "A two-current model for the dynamics of cardiac membrane," *Bulletin of mathematical biology*, vol. 65, no. 5, pp. 767–793, 2003.

[5] J. Relan *et al.*, "Personalization of a cardiac electrophysiology model using optical mapping and mri for prediction of changes with pacing," *Biomedical Engineering, IEEE Transactions on*, vol. 58, no. 12, pp. 3339–3349, 2011.

[6] ——, "Coupled personalization of cardiac electrophysiology models for prediction of ischaemic ventricular tachycardia," *Interface Focus*, 2011.

[7] M. Wallman, N. P. Smith, and B. Rodriguez, "Computational methods to reduce uncertainty in the estimation of cardiac conduction properties from electroanatomical recordings," *Medical image analysis*, vol. 18, no. 1, pp. 228–240, 2014.

[8] E. Konukoglu *et al.*, "Efficient probabilistic model personalization integrating uncertainty on data and parameters: Application to eikonal-diffusion models in cardiac electrophysiology," *Progress in biophysics and molecular biology*, vol. 107, no. 1, pp. 134–146, 2011.

[9] O. Dössel *et al.*, "A framework for personalization of computational models of the human atria," in *Engineering in Medicine and Biology Society, EMBC, 2011 Annual International Conference of the IEEE*. IEEE, 2011, pp. 4324–4328.

[10] O. Zettinig *et al.*, "Data-driven estimation of cardiac electrical diffusivity from 12-lead ecg signals," *Medical image analysis*, vol. 18, no. 8, pp. 1361–1376, 2014.

[11] D. U. Keller *et al.*, "Ranking the influence of tissue conductivities on forward-calculated ecgs," *IEEE Transactions on Biomedical Engineering*, vol. 57, no. 7, pp. 1568–1576, 2010.

[12] C. Ramanathan and Y. Rudy, "Electrocardiographic imaging: Effect of torso inhomogeneities on noninvasive reconstruction of epicardial potentials, electrograms, and isochrones," *Journal of cardiovascular electrophysiology*, vol. 12, no. 2, pp. 241–252, 2001.

[13] C. E. Chávez *et al.*, "Inverse problem of electrocardiography: Estimating the location of cardiac ischemia in a 3d realistic geometry," in *International Conference on Functional Imaging and Modeling of the Heart*. Springer, 2015, pp. 393–401.

[14] A. J. Pullan *et al.*, "The inverse problem of electrocardiography," in *Comprehensive Electrocardiology*. Springer London, 2010, pp. 299–344.

[15] G. Huiskamp and A. Van Oosterom, "The depolarization sequence of the human heart surface computed from measured body surface potentials," *Biomedical Engineering, IEEE Transactions on*, vol. 35, no. 12, pp. 1047–1058, 1988.

[16] S. Ghosh and Y. Rudy, "Application of l1-norm regularization to epicardial potential solution of the inverse electrocardiography problem," *Annals of Biomedical Engineering*, vol. 37, no. 5, pp. 902–912, 2009.

[17] B. Messnarz *et al.*, "A new spatiotemporal regularization approach for reconstruction of cardiac transmembrane potential patterns," *Biomedical Engineering, IEEE Transactions on*, vol. 51, no. 2, pp. 273–281, 2004.

[18] Y. Jiang, D. Farina, and O. Dössel, "Localization of the origin of ventricular premature beats by reconstruction of electrical sources using spatio-temporal map-based regularization," in *4th European Conference of the International Federation for Medical and Biological Engineering*. Springer, 2009, pp. 2511–2514.

[19] Z. Liu, C. Liu, and B. He, "Noninvasive reconstruction of 3d ventricular activation sequence from the inverse solution of distributed equivalent current density," *IEEE transactions on medical imaging*, vol. 25, no. 10, pp. 1307–1318, 2006.

[20] C. Han *et al.*, "Noninvasive imaging of 3d cardiac activation sequence during pacing and ventricular tachycardia," *Heart Rhythm*, vol. 8, no. 8, pp. 1266–1272, 2011.

[21] ——, "Noninvasive cardiac activation imaging of ventricular arrhythmias during drug-induced qt prolongation in the rabbit heart," *Heart Rhythm*, vol. 10, no. 10, pp. 1509–1515, 2013.

[22] ——, "Imaging cardiac activation sequence during ventricular tachycardia in a canine model of nonischemic heart failure," *American Journal of Physiology-Heart and Circulatory Physiology*, vol. 308, no. 2, pp. H108–H114, 2015.

[23] L. Yu, Z. Zhou, and B. He, "Temporal sparse promoting three dimensional imaging of cardiac activation," *IEEE transactions on medical imaging*, vol. 34, no. 11, pp. 2309–2319, 2015.

[24] H. S. Oster and Y. Rudy, "The use of temporal information in the regularization of the inverse problem of electrocardiography," *Biomedical Engineering, IEEE Transactions on*, vol. 39, no. 1, pp. 65–75, 1992.

[25] A. Rahimi Dehaghani *et al.*, "Examining the impact of prior models in transmural electrophysiological imaging: A hierarchical multiple-model bayesian approach," *IEEE transactions on medical imaging*, vol. 35, no. 1, pp. 229–243, 2016.

[26] L. Wang *et al.*, "Noninvasive computational imaging of cardiac electrophysiology for 3-d infarct," *Biomedical Engineering, IEEE Transactions on*, vol. 58, no. 4, pp. 1033–1043, 2011.

[27] G. Li and B. He, "Localization of the site of origin of cardiac activation by means of a heart-model-based electrocardiographic imaging approach," *IEEE transactions on biomedical engineering*, vol. 48, no. 6, pp. 660–669, 2001.

[28] B. He, G. Li, and X. Zhang, "Noninvasive three-dimensional activation time imaging of ventricular excitation by means of a heart-excitation model," *Physics in medicine and biology*, vol. 47, no. 22, p. 4063, 2002.

[29] X. Zhang *et al.*, "Noninvasive 3d electrocardiographic imaging of ventricular activation sequence," *American Journal of Physiology-Heart and Circulatory Physiology*, vol. 289, no. 6, pp. H2724–H2732, 2005.

[30] C. Liu *et al.*, "Estimation of global ventricular activation sequences by noninvasive 3d electrical imaging: Validation studies in a swine model during pacing," *Journal of cardiovascular electrophysiology*, vol. 19, no. 5, pp. 535–540, 2008.

[31] ——, "Noninvasive mapping of transmural potentials during activation in swine hearts from body surface electrocardiograms," *IEEE transactions on medical imaging*, vol. 31, no. 9, pp. 1777–1785, 2012.

[32] C. Ramanathan *et al.*, "Noninvasive electrocardiographic imaging (ecgi): application of the generalized minimal residual (gmres) method," *Annals of Biomedical Engineering*, vol. 31, no. 8, pp. 981–994, 2003.

[33] R. Dubois *et al.*, "Non-invasive cardiac mapping in clinical practice: Application to the ablation of cardiac arrhythmias," *Journal of Electrocardiology*, vol. 48, no. 6, pp. 966 – 974, 2015.

[34] N. Varma, P. Jia, and Y. Rudy, "Electrocardiographic imaging of patients with heart failure with left bundle branch block and response to cardiac resynchronization therapy," *Journal of electrocardiology*, vol. 40, no. 6, pp. S174–S178, 2007.

[35] S. Ghosh *et al.*, "Electrophysiologic substrate and intraventricular left ventricular dyssynchrony in nonischemic heart failure patients undergoing crt," *Heart Rhythm*, vol. 8, no. 5, pp. 692–699, 2011.

[36] F. Dawoud *et al.*, "Non-invasive electromechanical activation imaging as a tool to study left ventricular dyssynchronous patients: Implication for crt therapy," *Journal of electrocardiology*, vol. 49, no. 3, pp. 375–382, 2016.

[37] Z. Chen *et al.*, "Biophysical modelling predicts VT inducibility and circuit morphology," *Journal of Cardiovascular Electrophysiology*, 2016.

[38] M. Potse *et al.*, "A comparison of monodomain and bidomain reaction-diffusion models for action potential propagation in the human heart," *Biomedical Engineering, IEEE Transactions on*, vol. 53, no. 12, pp. 2425–2435, 2006.

[39] J. Malmivuo and R. Plonsey, *Bioelectromagnetism: principles and applications of bioelectric and biomagnetic fields*. Oxford university press, 1995.

[40] H. Delingette and N. Ayache, "Soft tissue modeling for surgery simulation," *Handbook of Numerical Analysis*, vol. 12, pp. 453–550, 2004.

[41] H. Talbot *et al.*, "Towards real-time computation of cardiac electrophysiology for training simulator," in *STACOM International Workshop*. Springer, 2012, pp. 298–306.

[42] J. Kybic *et al.*, "A common formalism for the integral formulations of the forward eeg problem," *Medical Imaging, IEEE Transactions on*, vol. 24, no. 1, pp. 12–28, 2005.

[43] L. G. Tereshchenko *et al.*, "A new electrocardiogram marker to identify patients at low risk for ventricular tachyarrhythmias: sum magnitude of the absolute qrst integral," *Journal of electrocardiology*, vol. 44, no. 2, pp. 208–216, 2011.

[44] W. H. W. Schulze, *ECG imaging of ventricular activity in clinical applications*, K. I. of Technology / Institute of Biomedical Engineering, Ed. Karlsruhe: KIT Scientific Publishing, 2015.

[45] A. Groth, J. Weese, and H. Lehmann, "Robust left ventricular myocardium segmentation for multi-protocol MR," in *SPIE Medical Imaging*. International Society for Optics and Photonics, 2012, p. 83142S.

[46] D. Durrer *et al.*, "Total excitation of the isolated human heart," *Circulation*, vol. 41, no. 6, pp. 899–912, 1970.

[47] D. J. Swenson *et al.*, "Cardiac position sensitivity study in the electrocardiographic forward problem using stochastic collocation and boundary element methods," *Annals of biomedical engineering*, vol. 39, no. 12, pp. 2900–2910, 2011.